Published online 3 August 2015

Nucleic Acids Research, 2015, Vol. 43, No. 19 ***9249–9261***
doi: 10.1093/nar/gkv788

The interaction of ω_2 with the RNA polymerase β' subunit functions as an activation to repression switch

Andrea Volante, Begoña Carrasco, Mariangela Tabone and Juan C. Alonso*

Department of Microbial Biotechnology, Centro Nacional de Biotecnología, CNB-CSIC, 3, Darwin Street, 28049 Madrid, Spain

Received May 12, 2015; Revised July 16, 2015; Accepted July 23, 2015

ABSTRACT

The ω gene is encoded in broad-host range and low-copy plasmids. It is genetically linked to antibiotic resistance genes of the major human pathogens of phylum Firmicutes. The homodimeric forms of ω (ω_2) coordinate the plasmid copy number control, faithful partition (ω_2 and δ_2) and better-than-random segregation ($\zeta\epsilon_2\zeta$) systems. The promoter (*P*) of the ωεζ operon (P_ω) transiently interacts with ω_2. Adding δ_2 facilitates the formation of stable $\omega_2 \cdot P_\omega$ complexes. Here we show that limiting ω_2 interacts with the N-terminal domain of the β' subunit of the *Bacillus subtilis* RNA polymerase (RNAP-σ^A) vegetative holoenzyme. In this way ω_2 recruits RNAP-σ^A onto P_ω DNA. Partial P_ω occupancy by ω_2 increases the rate at which RNAP-σ^A complex shifts from its closed (RP_C) to open (RP_O) form. This shift increases transcription activation. Adding δ_2 further increases the rate of P_ω transcription initiation, perhaps by stabilizing the $\omega_2 \cdot P_\omega$ complex. In contrast, full operator occupancy by ω_2 facilitates RP_C formation, but it blocks RP_O isomerization and represses P_ω utilization. The stimulation and inhibition of RP_O formation is the mechanism whereby ω_2 mediates copy number fluctuation and stable plasmid segregation. By this mechanism, ω_2 also indirectly influences the acquisition of antibiotic resistance genes.

INTRODUCTION

Resistance to glycopeptides, macrolides, pleuromutilins, phenicols, linezolid and other antibiotics among Gram-positive cocci is generally linked to plasmids whose copy number control, partitioning and post-segregational killing is regulated by the ω cassette (1,2). This cassette contains sequences that encode the ω or ω2 gene products (1). It is thus important to understand how homodimeric ω (ω_2) (or ω2 [$\omega 2_2$]) functions, not only because of its intrinsic biological interest, but also because of its relevance to antibiotic resistance transmission (1,2). Plasmids of the *inc*18 family are commonly found in *Enterococcus* and *Streptococcus*. These plasmids have a broad host range in Firmicutes. Here, ω forms an operon with ε and ζ. Meanwhile, ω2 forms an operon with the *ermB* gene (1).

A transcriptional analysis of few *inc*18 plasmids (e.g. pSM19035, pIP501 and pAMβ1) revealed that ω_2 controlled the expression of the copy control gene *copS*. Also mediated by ω_2 was the expression of plasmid partition genes, such as δ and ω, and toxin-antitoxin systems, such as the ωεζ operon (Figure 1A) (1). The *inc*18 plasmids persist in the population through a variety of mechanisms controlled by ω_2. The ω_2 protein is a ParB homologue and binds to *parS* centromers. In concert with δ_2 (a ParA ATPase), ω_2 is involved in accurate plasmid partitioning and coupling plasmid replication to faithful segregation (1,3–5). All three *parS* sites (Figure 1A) can cause partition-mediated incompatibility (5). Furthermore, toxin ζ stabilizes bacterial plasmids by programming the death of any host cell that fails to inherit a plasmid copy during cell division (1,6). Toxins ζ and RelE are the most ubiquitous toxins in nature. In contrast, much less is known about the purpose of the ω2 gene product, which is truncated in some members of the family (e.g. pSM19035) (Figure 1A) (1).

Streptococcus pyogenes monomeric ω (71-residue long, 7.9 kDa) has an unstructured N-terminal domain (NTD, residues 1–24) followed by a ribbon-helix-helix (RHH) fold (residues 25–71). The latter facilitates the formation, in solution, of a dimer that has a pseudo-2-fold symmetry (7–9). The RHH domain recognizes the *parS* centromers embedded in the promoter regions of the *cop*, δ, ω and ω2 genes (Figure 1A and Supplementary Figure S1) (4). The operator binding sites are comprised of a series of 6–10 unspaced heptad repeats (5′-$^{T}/_{A}$ATCAC$^{T}/_{A}$-3′) in a forward orientation. Alternatively, they consist of two or three repeats of the following: two heptads in a forward orientation followed by one in an inverse orientation (→→←) (Supplementary Figure S1). Both the ω_2 and the NTD lacking $\omega_2\Delta$N19 mutant

*To whom correspondence should be addressed. Tel: +34 91585 4546; Fax: +34 91585 4506; Email: jcalonso@cnb.csic.es

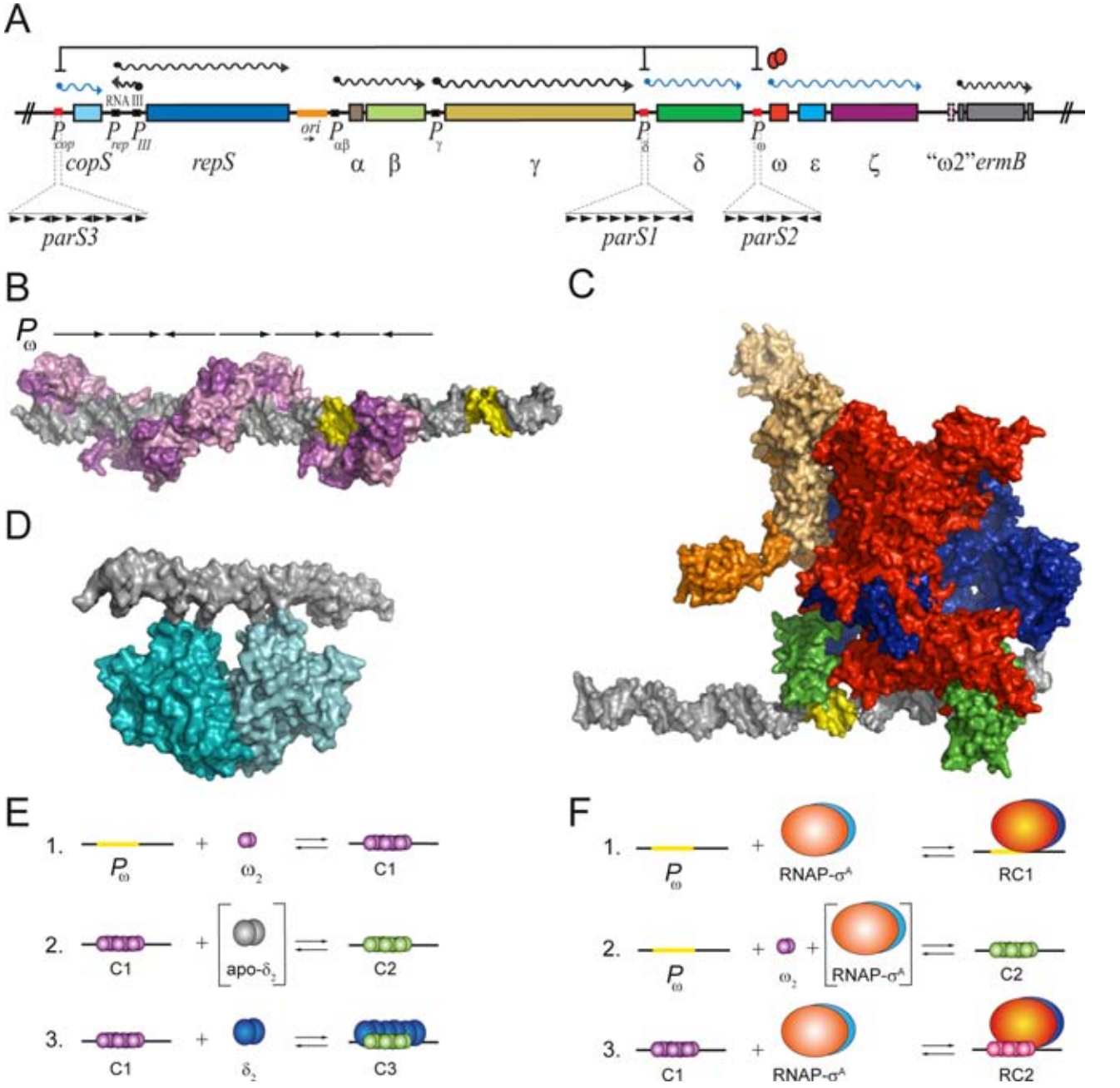

Figure 1. Interaction of ω_2, δ_2 or RNAP-σ^A with the P_ω operator sites. (**A**) Genome organization of the relevant region of plasmid pSM19035. The promoters (*P*), the mRNAs and the genes are symbolized by boxes, wavy lanes and rectangles, respectively. The plasmid replication origin (*ori*) is labelled in orange. The direction of replication is denoted by a black arrows below. Protein ω_2-mediated transcriptional repression is indicated (ω_2, red ovals). The upstream regions of P_{copS}, P_δ and P_ω (red box) which constitute the *cis*-acting *parS* centromeric sites magnified. The ω_2 cognate sites consist of a variable number of contiguous 7-bp heptad repeats (iterons) symbolized by ► (in the direct orientation) or ◄ (in the inverted orientation). The number of repeats and their relative orientations are indicated. The genes involved in replication (*copS*, *repS,* RNAIII and γ), dimer resolution (β), faithful partition (δ and ω), stable segregation (ϵ and ζ) are indicated. The antibiotic resistance gene *ermB* and the truncated version of ω2 ('ω2') are also indicated. (**B**) A structural model of ω_2-bound to P_ω DNA which derived from the crystal structure of the complex of the minimal operator site and $\omega_2\Delta19$ (PDB ID 1IRQ, 2BNW and 2BNZ). Pink/purple ω_2 molecules form a left-handed protein-matrix winding around the nearly linear operator DNA. The DNA is represented in grey with the −35 and −10 elements in yellow. (**C**) Model of RNAP-σ^A which is derived from crystal structures of the homologous protein from *T. aquaticus* and *T. thermophilus* (PDB ID 1IW7, 2A6H) together with the P_ω DNA from PDB ID 2CAX. Colour coding: brown and light brown refer to α_2; blue, β; red, β' and green, σ subunit. (**D**) Model of δ_2 binding to DNA. The atomic coordinates of $(\delta{\cdot}ATP\gamma S{\cdot}Mg^{2+})_2$ were taken from the 2OZE PDB entry. The modelled structures were prepared and visualized with PyMOL version 1.5.0.4. (**E**) Interactions of ω_2 and δ_2 with P_ω DNA and each other: 1. ω_2 (in purple) transiently interacts with P_ω DNA forming complex C1; 2. The interaction of ω_2 with δ_2-apo (in grey), leads to functional transition of ω_2 (in green) and formation of the durable C2 complex; 3. In the presence of ATP, δ_2 (in blue) binds to C1 to generate C3. (**F**) Complexes formed by ω_2 and RNAP-σ^A upon binding to P_ω DNA: 1. RNAP-σ^A bound to P_ω DNA forms complex RC1; 2. the interaction of RNAP-σ^A with limiting concentrations of ω_2 leads to a functional transition of ω_2 and formation of C2; and 3. RNAP-σ^A bound to C1 makes RC2.

transiently bind promoters and repress promoter utilization both *in vivo* and *in vitro* (4,9–13).

The minimal ω_2 binding site is comprised of two contiguous heptads in a forward (→→) or inverted (→←) orientation. It has higher affinity for the latter (see 10). The structure of the complex of ω_2 bound to →→ DNA is very similar to the one of ω_2 bound to →← DNA. In neither case does ω_2 distort the DNA when binding to it (9,14). These structures show that a pair of positively charged antiparallel β strands from ω_2 insert into the major groove of DNA. The β strands make specific and sequence-dependent contacts with symmetric or asymmetric repetitive sequences that deviate 0.3 Å with respect to the central C-G pair of each repetition (8,9,14). In a full cognate site, ω_2 is displaced ∼7-bp and rotated 252° with respect to its neighbouring dimer. The negatively charged sugar-phosphate DNA backbone faces the positively charged surface of the protein (Figure 1B) (9).

Protein ω_2 transiently binds with high affinity (apparent dissociation constant $[K_{Dapp}] = 5 \pm 1$ nM) and cooperativity to P_ω DNA (Figure 1E, condition 1 [C1]) (13). The physical interaction of the apo form of δ_2 with ω_2 bound to P_ω DNA facilitates a structural transition in ω_2 that might involve folding of its unstructured NTD (Figure 1E, condition 2) (see 13,15). ω_2 stably binds P_ω DNA with high affinity ($K_{Dapp} = 0.7 \pm 0.1$ nM), forming the C2 complex ($\omega_2 \cdot P_\omega$ DNA) (Figure 1E, condition 2). The C2 complex is stable, with a half-life of >30 min, whereas the C1 complex is transient, with half-life of <1 min (10,13,15). However, despite the difference in stability, C1 and C2 have a similar mobility in a PAGE at low protein concentrations.

The δ_2 protein is a U-shaped ATPase that in its ATP-bound form, binds non-specifically to DNA (Figure 1D) (16). In the presence of ATP, δ_2 interacts with C1 to form the C3 complex (Figure 1E, condition 3) (13). Since it lacks the unfolded NTD, $\omega_2\Delta$N19 cannot facilitate C2 and C3 formation (13). Given that δ_2 (a ParA ATPase) works together with ω_2 (a ParB centromeric binding protein) bound to *parS* (e.g. P_ω DNA) to promote faithful plasmid segregation (12,13), it is likely that δ_2 also contributes to ω_2-mediated transcription regulation.

Transcription initiation by the multisubunit RNA polymerase (RNAP) is an intricate multistep process (17–20). Bacterial RNAP exists in two forms: i) the ubiquitous core enzyme, which consists of the dimeric form of α (α_2), the monomeric form of β, β', and one or more of small non-essential subunits; this carries out processive transcription elongation followed by termination; and ii) the RNAP-σ holoenzyme, in which a dissociable σ subunit, essential for promoter recognition, has joined the core enzyme (21–23). The *Bacillus subtilis* vegetative RNAP-σ^A holoenzyme binds to specific −10 and −35 promoter (*P*) elements to form an unstable closed binary complex (RP_C) (21,24–27). A RNAP-σ^A-assisted isomerization step then occurs. This is mediated by kinetically unstable intermediates (RP_I). This, in turn, leads to *P* melting of ∼14-bp (−12 to +2) in the DNA surrounding the transcription start site. This process yields the catalytically active, open RNAP-$\sigma^A \cdot P$ DNA complex (RP_O) (17,28). The structures responsible for the functions associated with RPo formation are predominantly located in the σ, β and β' subunits of the RNAP-σ (18,22,23,25,28). In the presence of nucleotide triphosphates, an initiation complex (RP_{INIT}) is formed. This complex is a prerequisite for displacement of RNAP-σ^A from the promoter through an elongation complex (RP_E) (24,25,28). RNAP subunits δ, ϵ and ω are not essential for this process and their roles are therefore poorly understood.

As a result of the association of regulatory elements to promoter-embedded operator sequences, gene regulation is often achieved at the level of transcription initiation (29). The ω_2 protein interacts with its cognate sites as a left-handed protein helix wrapped around a nearly linear P_ω DNA (9). In this structure the −35 and −10 elements are free to interact with RNAP-σ^A (Figure 1B, yellow regions). A model of RNAP-σ bound to P_ω DNA suggests that ω_2 might repress transcription by steric hindrance (Figure 1C). However, preliminary results indicate that ω_2 forms a ternary complex with RNAP-σ^A and P_{copS} DNA (4). These data suggest that ω_2 regulates transcription through a mechanism that does not exclude the RNAP-σ^A from the RP_C. It is assumed that this mechanism also applies to P_ω and P_δ. In this study, we aimed to unravel the mechanism of ω_2-mediated transcriptional regulation of P_ω DNA, *in vitro*, and P_δ utilization, *in vivo*. We first characterized the effect that ω_2 binding to P_ω DNA had on RNAP-σ^A promoter recognition. We also tested whether or not modifying the stoichiometry of ω_2, δ_2 and RNAP-σ^A resulted in variations in their affinity for P_ω DNA. Also investigated was whether or not transcription activation or repression by ω_2 required direct contacts with RNAP-σ^A and δ_2. Another important question was whether or not this binding was cooperative. Based on the results of this study, we present a model that explains how ω_2-mediated transcriptional regulation functions.

MATERIALS AND METHODS

Bacterial strains and plasmids

The *E. coli* strains DH5α (Invitrogen) and ER2566 (New England Biolabs) and the *B. subtilis* strains BG214, BG508 (4) and NIG2001 (30) were used. The BG508 strain carries P_δ fused to a promoter-less *lacZ* gene. This construct was integrated as a unique copy into the *amyE locus* of the *B. subtilis* chromosome (4). In the NIG2001 strain, the wild-type (wt) *rpoC* gene was substituted in the *B. subtilis* genome with a version that had a His-tag coding sequence fused to the 3′-end (30). The P_ω bearing pCB30 plasmid was used for promoter analysis, and pHP14 was used for cloning purposes (4). The plasmids used for gene over-expression were pT712ω bearing ω, pCB746 bearing δ (4,11,16), and pT712ωD56A bearing the ωD56A gene (this work). The single mutations in the ω gene were obtained by gene synthesis (Genscript). BG508 cells bearing pHP14 carrying either the ω, δ, ωδ, ωΔN19, ω2, ωK52A, ωE53A, ωD56A, ωR64A or ωK70A genes were used for the β-galactosidase assays. The native promoters of these genes were also incorporated into the constructs.

DNA, RNA, proteins and reagents

Plasmid DNA was purified as described (4). The multiple mutations in heptads 1, 1 plus 2, 7 and 7 plus 6 were ob-

tained by *in vitro* synthesis (Genscript). DNA restriction and modification enzymes and RNaseA were purchased from Boehringer Mannheim and the nucleotides were purchased from Sigma. Gel-purified DNA fragments were end-labelled as described (4). The amount of DNA was quantified using molar extinction coefficient of 6500 M^{-1} cm^{-1} at 260 nm and was expressed in moles of DNA molecules.

The RNAP-σ^A was purified using Ni-NTA and Q-sepharose columns as described (30). The ω_2 and δ_2 proteins were purified as described (4,11,16). Protein ωD56A was purified as wt ω_2. Protein concentrations were calculated using molar extinction coefficients at 280 nm of 2980, 2980, 38 850 and 236 000 M^{-1} cm^{-1} for ω_2, ωD56A, δ_2, and RNAP-σ^A, respectively. Concentrations were expressed in molarity of protein monomers for RNAP-σ^A and of dimers for δ_2, ω_2 and ω_2 derivatives. Note that unless otherwise stated, δ_2 is in the ATP·Mg^{2+}-bound form.

B. subtilis BG508 harbouring different plasmids was grown to OD_{600} = ∼0.5 and aliquots were used for β-galactosidase assays (4). The cultures were pelleted and resuspended in buffer B (10 mM Na_2HPO_4/NaH_2PO_4 pH 7.2, 50 mM β-mercaptoethanol, 1 mM $MgCl_2$, 10 mM KCl) containing 0.4 μg/ml lysozyme (4). After a 5 min incubation at 37°C, the lysates were clarified by centrifugation for 5 min at 12,000 *g* and assayed for β-galactosidase activity, as described (31).

Protein cross-linking was used to study potential protein–protein interactions. For this, *bis*disuccinimidyl suberate (DSS) was employed as the crosslinking agent and SDS-PAGE was used to visualize the result (13). Two-dimensional gel electrophoresis (2D) was performed essentially as described (32). The resolved proteins were transferred onto a 0.45 μm polyvinylidene fluoride membrane (PVDF, Millipore). Rabbit polyclonal anti-ω_2 and anti-RNAP-σ^A antibodies were obtained using standard techniques (4).

Far-western blotting was used to probe the direct interaction between ω_2 and RNAP-σ^A. The prey used were ω_2 (1 μg), RNAP-σ^A (1 μg) and bovine serum albumin (BSA, 5 μg used as a control); these were resolved by SDS-PAGE and transferred to a PVDF membrane. The protein was renatured by incubation of the membrane in TBS containing 0.05% Tween, 10% glycerol and 5 mM β-mercaptoethanol followed by a blocking step with 5% skim milk, as described (4). The efficiency of the protein transfer was checked by Ponceau staining. The membrane was then incubated with 2 μg/ml of bait protein. To detect interactions between the bait and prey, rabbit polyclonal antibodies against the bait were employed as described (33).

Tryptic digestion of gel-purified protein bands, spotting onto the MALDI-targets, and MALDI-TOF-TOF of the spotted peptides were carried out as previously described (34).

In vitro transcription experiments

A 423-bp P_ω DNA sequence (5 nM) was used as a template for *in vitro* transcription run-off assays. 20 μl reaction mixtures containing 20 nM *B. subtilis* RNAP-σ^A, variable concentrations of ω_2, δ_2 or both, 0.5 mM each of ATP, CTP, GTP and UTP plus 3000 Ci/mmol [α-^{32}P]-UTP in buffer C (25 mM Tris-HCl, pH 8, 6 mM MgOAc, 5 mM DTT), and 20 U RNasin (Promega) were prepared. After 6 min of incubation at 37°C, the reactions were stopped by adding 10 μl of formamide. RNAs were analysed by 8% denaturing (d) polyacrylamide gel electrophoresis (PAGE), and autoradiographed. Chemical sequencing reactions of the purines were run in parallel to determine the sizes of the cDNAs.

Protein-DNA complexes

For electrophoretic mobility shift assays (EMSA), the 423-bp [α^{32}P]-P_ω DNA (0.1 nM) was incubated either with a variety of concentrations of ω_2, δ_2 or RNAP-σ^A or with a constant concentration of one component and a range of concentrations of the others. Incubations were performed in buffer D (50 mM Tris-HCl pH 7.5, 50 mM NaCl, 10 mM $MgCl_2$) for 15 min at 37°C in a 20 μl reaction. Mixtures were subjected to 6% PAGE in 1xTAE at 4°C. Gels were dried prior to autoradiographical analysis.

In order to obtain K_{Dapp} values from the EMSA experiments, the relative concentrations of free DNA and protein·DNA complexes were densitometrically determined under non-saturating conditions using differently exposed autoradiographs of the EMSA gels. The protein concentration needed to trap 50% of the free, labelled DNA containing the same molar concentration of heptads, in complexes is approximately equal to the K_{Dapp} under conditions where the DNA concentration is much lower than the K_{Dapp}.

Reaction conditions similar to those used for EMSA were employed in footprinting experiments. The 423-bp [α^{32}P]-P_ω DNA (1 nM) was incubated with variable protein concentrations and treated with DNaseI, as previously described (4). The samples were resolved by 6% dPAGE and the gel was dried prior to autoradiographical analysis. For $KMnO_4$ footprinting, the samples were treated with 1 mM $KMnO_4$ for 0.5 min at 37° C, after which the DNA was cleaved with piperidine (35).

RESULTS

RNAP-σ^A facilitates $\omega_2 \cdot P_\omega$ DNA complex formation

In order to unravel the mechanism of ω_2-mediated regulation of P_ω utilization, the interaction of ω_2 and/or RNAP-σ^A with P_ω DNA was assayed by EMSA (Figure 2A and 2B). P_ω DNA has 7 discrete ω_2 cognate sites. A 423-bp DNA segment containing P_ω bound ω_2 with high affinity to form $\omega_2 \cdot P_\omega$ DNA also known as the C1 complex (K_{Dapp} of 6 ± 1.7 nM) (Figure 2C filled circles). When P_ω DNA was replaced with a non-specific DNA, the affinity of ω_2 was low, with a K_{Dapp} > 500 nM (data not shown) (4). This confirmed previously reported data indicating a high affinity of ω_2 for P_{copS}, P_δ and P_ω (10). In addition, binding was found to be cooperative (Figure 2C). P_ω also bound RNAP-σ^A with high affinity to form RNAP-$\sigma^A \cdot P_\omega$ DNA, also known as the RC1 complex (K_{Dapp} of 29.4 ± 9 nM, Figure 2C filled rombs).

In the presence of limiting ω_2 (0.75 nM) concentrations, $\omega_2 \cdot P_\omega$ DNA complex formation was not observed (Figure 2A, lane 2 and 2C filled circles). Increased concentra-

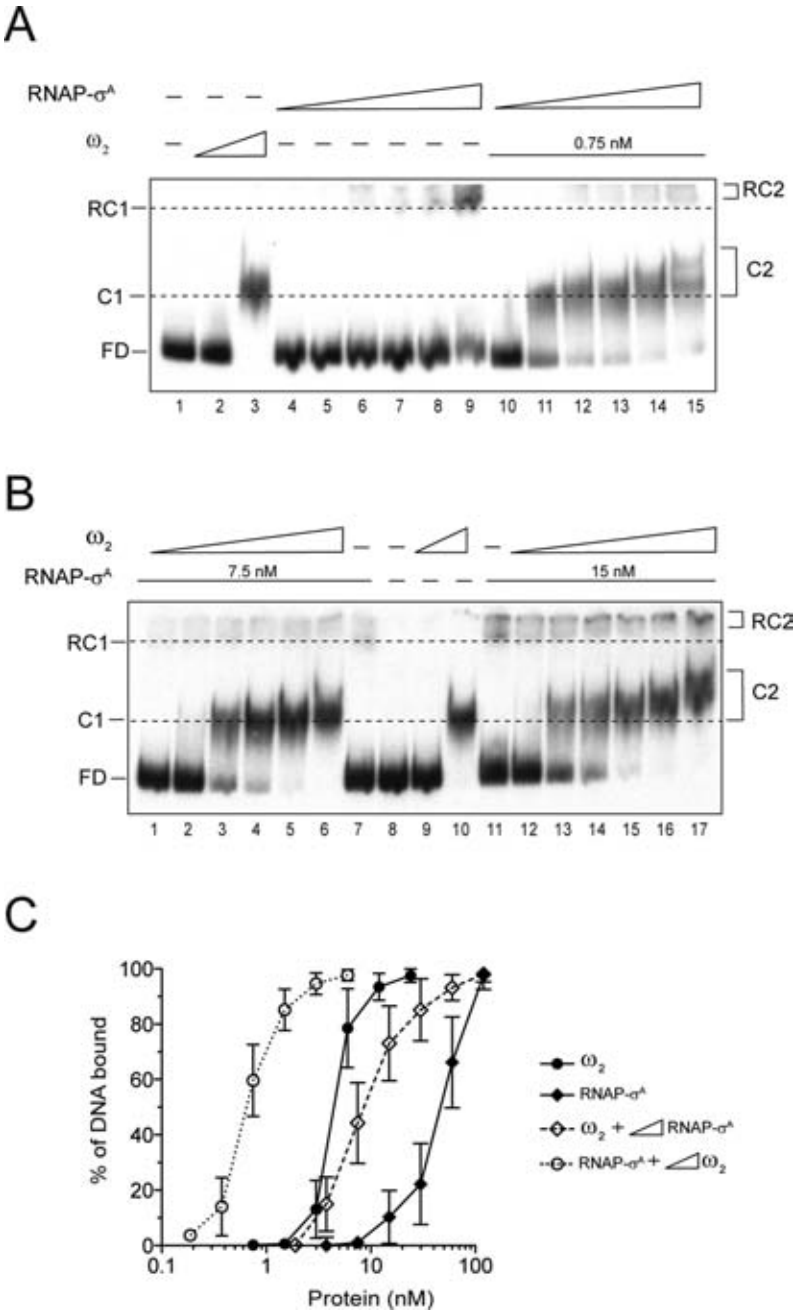

Figure 2. Cooperative binding of ω_2 and RNAP-σ^A to P_ω DNA. (**A**) EMSA of (0.1 nM) 423-bp [α^{32}P]-P_ω DNA incubated with 0.75 nM and 6 nM ω_2 (lanes 2 and 3), increasing concentrations of RNAP-σ^A (1.9, 3.7, 7.5, 15, 30 and 60 nM, lanes 4–9), or fix ω_2 (0.75 nM) and increasing concentrations of RNAP-σ^A (1.9–60 nM) (lanes 10–15) in buffer D. (**B**) EMSA of [α^{32}P]-P_ω DNA with of 0.75 nM and 6 nM ω_2 (lanes 9 and 10, respectively) or with 7.5 nM (lanes 1–7) or 15 nM (lanes 11–17) RNAP-σ^A and increasing concentrations of ω_2 (0.19, 0.37, 0.75, 1.5, 3 and 6 nM) in buffer D. (**C**) Graph showing the percentage of P_ω DNA bound to the proteins based on densitometric data of bands from the above gels. The signals present in the protein-DNA complex and in the free-DNA (FD) were determined by densitometry. The data presented here are averages and standard deviations of the results of at least four independent experiments.

tions of RNAP-σ^A enhanced recruitment of ω_2 to the promoter region by at least 8-fold. This was observed as an increase in the formation of high affinity C2 complexes. This effect was detected using limiting RNAP-σ^A concentrations (3.7 nM) (Figure 2A, lanes 11–15). The 'cooperative' binding leading to C2 complex formation could not be attributed to molecular crowding, because the BSA control did not function as a substitute for RNAP-σ^A (data not shown). The stable C2 and the transient C1 had a similar mobility. However, at higher concentrations of ω_2, the mobility of C2 was even further diminished (Figure 2A, lanes 3 versus 11). The C1 complex had a half-life of <1 min (10). The formation of the $\omega_2 \cdot P_\omega$ DNA complex was also enhanced at least 8-fold (K_{Dapp} of 0.6 ± 0.2 nM) when a

fixed limiting concentration of RNAP-σ^A (~4-fold below K_{Dapp}) and increasing concentrations of ω_2 were incubated with P_ω DNA (Figure 2B, lanes 1–6 and 2C open circles).

To distinguish cooperative binding from a mechanism whereby a protein–protein interaction preceded binding to P_ω DNA, the experiment was modified by doubling the concentration of RNAP (~2-fold below K_{Dapp}). In the presence of sub-stoichiometric concentrations of RNAP-σ^A (15 nM), the $\omega_2 \cdot P_\omega$ DNA complex formation became enhanced by at least 10-fold. This resulted in a stoichiometry of ~2 ω_2/P_ω DNA (Figure 2B, lanes 12–17 and 2C, open circles). This is consistent with the known characteristics of ω_2 binding to P_ω DNA which had a stoichiometry of ~1 ± 0.2 ω_2 /heptad. The minimal ω_2 binding site consisted of two contiguous heptads (9–12). It is therefore likely that ω_2 interacts with RNAP-σ^A, and that such an interaction induces a conformational change in the former that increases its apparent affinity for P_ω DNA. This favours the formation of the C2 complex. Meanwhile, in the absence of RNAP-σ^A, ω_2-bound to P_ω forms the C1 complex with an 8-fold lower apparent affinity (K_{Dapp} of 6 ± 1.7 nM).

A low concentration of ω_2 facilitates the formation of the RNAP-$\sigma^A \cdot P_\omega$ DNA complex

Limiting concentrations of ω_2 enhanced the recruitment of RNAP-σ^A to P_ω DNA (Figure 2B, lanes 1–3 and 12–14). 7.5 nM RNAP-σ^A was the limiting concentration of RNAP-σ^A necessary to detect the RC2 complex (RNAP-$\sigma^A \cdot P_\omega$ DNA$\cdot\omega_2$). This was ~4-fold less than the K_{Dapp} (Figure 2C open versus filled rombs). It is therefore likely that ω_2 interacts with RNAP-σ^A and facilitates a functional transition of RNAP-σ^A. To test whether or not ω_2 and RNAP-σ^A co-localize in a RC2 complex, ω_2 and RNAP-σ^A were incubated with P_ω DNA and subjected to DNase I footprinting analysis. The ω_2 protein protected nucleotides −22 to −75 (with a numbering relative to the +1 transcription start site) (Supplementary Figure S2A, lanes 4–5). Meanwhile, RNAP-σ^A made a weak but significant contact with a segment located between positions −53 to +18. In parallel, a clearly hypersensitive site appeared at position −37. This is denoted by a dotted line square in Supplementary Figure S2A, lanes 6–9. Addition of a limiting concentration of ω_2 of ~4-fold below the K_{Dapp} resulted in the disappearance of the hypersensitive site. This effect was reversed upon increasing the concentration of RNAP-σ^A (Supplementary Figure S2A, lanes 10–13). It was also reversed by increasing the concentration of ω_2 to ~2-fold below the K_{Dapp} (Supplementary Figure S2B, lanes 13–16). Judging by the fading out of the hypersensitive site at position −37, it is likely that limiting concentrations of ω_2 or RNAP-σ^A reposition RNAP-σ^A on the P_ω DNA.

Addition of sub- to stoichiometric concentrations of ω_2 led to an increase in the formation of RC2 (RNAP-$\sigma^A \cdot P_\omega$ DNA$\cdot\omega_2$) complex formation by at least 3-fold (K_{Dapp} of 9.5 ± 3.4 nM) (Figure 2B, lane 17 and 2C, open rombs). Equilibrium was thus reached at about ~4 ω_2/RNAP-σ^A/P_ω DNA. These results suggested that there was not a sufficient number of ω_2 molecules to occupy the seven P_ω heptads. Since ω_2 binds with a slightly higher affinity and cooperativity to heptad pairs in the →← than in the →→ orientation (10), we favour the hypothesis that the →← heptads at positions −41 to −27, which overlap the −35 element and its neighbours, might be the ones recruited by ω_2 to interact with RNAP-σ^A. Indeed, sub- to stoichiometric concentrations of ω_2 bound to P_ω DNA protected this region from DNase I attack (Supplementary Figure S2B, lanes 3–6). Meanwhile at stoichiometric concentrations RNAP-σ^A made weak but extensive contacts with the upstream region, which had the same exposed hypersensitive site at position −37 (Supplementary Figure S2B, lanes 8–11). At sub-stoichiometric concentrations of ω_2, RNAP-σ^A made extensive contacts with the upstream −35 region. The hypersensitive site at position −37 remained exposed (Supplementary Figure S2B, lanes 13–16). This hypersensitive site was lost in the presence of stoichiometric concentrations of ω_2. Meanwhile, protection from DNase I was only observed in a stretch of DNA between positions −72 to −21 (Supplementary Figure S2B, lanes 18–21). In light of these results, it is likely that: (i) ω_2 physically interacts with RNAP-σ^A; and (ii) depending on the experimental conditions, ω_2 either displaces RNAP-σ^A from or re-localises with it on P_ω DNA.

The interaction between ω_2 and δ_2 does not affect RNAP-σ^A binding to P_ω DNA

Protein δ_2 bound non-specific DNA (K_{Dapp} 130 ± 20 nM) in the presence of ATP. This lead to the formation of the DC complex (Supplementary Figure S3A, lanes 6–8) (13). Binding of δ_2 to non-specific DNA increased 3 to 4-fold in the presence of $\omega_2 \cdot P_\omega$ DNA (Supplementary Figure S3A, lanes 10–12, and S3C, empty squares). In the absence of ATP, δ_2 only augmented the affinity of ω_2 for P_ω DNA by 6- to 10-fold (C2 formation) (Supplementary Figure S3B, lanes 10–15 and Figure 1E, condition 2). This was consistent with observations that: (i) the presence of apo-δ_2 decreased the off rate of ω_2 from $\omega_2 \cdot P_\omega$ DNA complexes; (ii) the presence of ω_2 significantly increased the half-life of the $\delta_2 \cdot P_\omega$ DNA complexes in the presence of ATP (13); and (iii) upon interacting with δ_2, ω_2 that is bound to P_ω DNA (*parS*) undergoes a structural transition that might involve the formation of an α-helix in the normally unstructured NTD (see 15).

To test whether the interaction of ω_2 with δ_2 or RNAP-σ^A are mutually exclusive or if the interaction between δ_2 and ω_2 affects ω_2-mediated recruitment onto the P_ω DNA of RNAP-σ^A, limiting concentrations of ω_2 (~8-fold below K_{Dapp}) and/or RNAP-σ^A (~4-fold below K_{Dapp}) were incubated with increasing δ_2 concentrations and subjected to an EMSA (Supplementary Figure S3A and S3B, lanes 10–15). In the presence of ATP, assembly of the ternary C3 complex ($\delta_2 \cdot \omega_2 \cdot P_\omega$ DNA) occurred (Supplementary Figure S3A, lanes 10–15). However, these results were not observed when ATP was omitted (Supplementary Figure S3B, lanes 10–15). Meanwhile, assembly of the ternary RC2 complex ($\omega_2 \cdot P_\omega \cdot$RNAP-$\sigma^A$) was observed without ATP (Supplementary Figure S3A and S3B, lanes 13–15). Finally, in the presence of ATP, δ_2 did not significantly affect the affinity of RNAP-σ^A for P_ω in the presence of ATP (Supplementary Figure S3D, lanes 8–16).

Whether ω_2 functions as an activator or repressor is dependent on its concentration

Protein ω_2 binds P_{copS}, P_δ and P_ω DNA with a stoichiometry of ~1 ± 0.2 ω_2 /heptad (9,12). We previously mapped the pSM19035 transcription start sites of P_{copS}, P_δ and P_ω (see Supplementary Figure S1). In that study, we showed that 7.5 – 15 ω_2/P_{copS}, P_δ or P_ω DNA represses promoter utilization (4). To gain insight into the mechanism by which ω_2 regulates promoter utilization, we performed transcription run-off experiments using RNAP-σ^A (at K_{Dapp}) in the presence of increasing concentrations of ω_2. Linear P_ω DNA containing seven heptads was used as the template (Figure 3A). As expected, 282-nt mRNA transcripts were produced (Figure 3B, lane 1). This result is consistent with the location of the initial nucleotides of P_ω, which had been previously mapped *in vivo* (4).

In the presence of limiting concentrations of ω_2 (0.9 and 1.8 ω_2/P_ω DNA), transcriptional activation was modest (1.4- to 1.7-fold), but reproducible (Figure 3B, lanes 2–4, and 3C). Protein ω_2 might preferentially bind the heptads of the P_ω DNA overlapping the −35 element. To test this hypothesis, the heptad 7, heptads 6 plus 7 and, as controls, heptads 1 or 1 plus 2 were inactivated (Figure 3A). As documented in Supplemental material Annex 1, the selective occupancy of heptads 6 and 7 versus 1 and 2 plays a minor role, if at all, in ω_2-mediated activation of P_ω utilization.

Stoichiometric concentrations of 7.5 ω_2/P_ω DNA inhibited P_ω expression by 4- to 8-fold. At slightly saturating conditions (15 ω_2/P_ω DNA or ~2 ω_2/heptad) mRNA synthesis halted completely (>50-fold) (Figure 3B, lanes 5 and 6). Concentrations of ω_2 equal to or higher than those required to repress P_ω did not affect the expression of the unrelated promoter (P_{cro} of phage A2) (data not shown). We could hence rule out RNase contamination or any other nonspecific effect as the reason for the lack of RNA synthesis. It is therefore likely that ω_2 has a dual activity: at limiting concentrations it facilitates the P_ω-RNAP-σ^A interaction, but at stoichiometric concentrations and higher, transcriptional repression results.

Limiting concentrations of ω_2 facilitate the transition from RP_C to RP_O and stoichiometric concentrations of ω_2 block this shift

To discern the mechanism of ω_2-mediated repression of P_ω, we investigated RP_O complex formation and abortive initiation (RP_{INIT}) effects in the presence of variable concentrations of ω_2. For this, we carried out $KMnO_4$ footprinting assays in the presence or absence of GTP and ATP. Up to 9-nt long transcripts were synthesized in these assays (see Supplementary Figure S1).

No oxidized thymines were detected on the template strand after 50 s of $KMnO_4$ exposure (Figure 4, lanes 1, 7, 13 and 19). In the absence of nucleotide precursors, the position in the P_ω DNA of non-base-paired thymines preferentially attacked by $KMnO_4$ revealed that RNAP-σ^A promoted spontaneous formation of a RP_O complex centred at position −11T and −10T of the template strand, rather than an extended *P* melting of ~14-bp (from −12 to +2) (Figure 4, lanes 2 and 8). $KMnO_4$-promoted cleavage of RNAP-σ^A bound template increased in the presence of sub-stoichiometric concentrations of ω_2 (Figure 4, Supplementary Figure S4A, lanes 3–4). Cleavage was inhibited at saturating concentrations of ω_2 (Figure 4, Supplementary Figure S4A, lanes 5–6). However, increased cleavage was not observed when sub-stoichiometric ω_2 concentrations were added to reactions containing RNAP-σ^A, i.e. with a preformed RP_O (Figure 4, lanes 9–10).

In the presence of ATP and GTP, RNAP-σ^A promoted abortive initiation and synthesis of up to 9-nt oligonucleotides (RP_{INIT}) (data not shown). $KMnO_4$ attack revealed the formation of an extended single-stranded bubble that cleaved at positions −10T, −6T, −5T and +7T (Figure 4, lanes 14 and 20). When ω_2 and RNAP-σ^A were left out, no cleavage was observed (Figure 4, lanes 13 and 19). Pre-incubation of P_ω DNA with sub-saturating concentrations of ω_2 followed by addition of RNAP-σ^A resulted in a significant increase (~2.5-fold) in $KMnO_4$ cleavage (Figure 4, lane 15 and 21 and Supplementary Figure S4B). At higher ω_2 concentrations, the reaction became inhibited (Figure 4, lanes 17–18, Supplementary Figure S4A, lanes 15–16 and S4B). However, RNAP-σ^A-mediated RP_O formation was hardly, if at all, affected by addition of ω_2 to the preformed RNAP-σ^A·P_ω complexes (Figure 4, lanes 21–24).

Altogether, these data suggest that: (i) ω_2 does not repress transcription by sterically hindering the interaction between RNAP-σ^A and P_ω DNA; (ii) in the absence of the nucleotides cofactors, RNAP-σ^A forms a short RP_O complex on P_ω centred at position −11T and −10T; (iii) limiting concentrations of ω_2 push RP_O to begin RNA synthesis (RP_{INIT}); (iv) stoichiometric concentrations of ω_2 inhibit RP_O formation, with ω_2 blocking the isomerization of RP_C to RP_O; and (v) ω_2 has no apparent effect on pre-formed RP_O. We cannot rule out that saturating concentrations of ω_2 may inhibit transcription by steric occlusion or relocation of RNAP-σ^A on preformed ω_2·P_ω complexes (see Supplementary Figure S2B, lanes 18–21).

Protein δ_2 represses P_ω expression

In the presence of ATP, δ_2 binds non-specific DNA with a K_{Dapp} = 130 ± 20 nM) (Supplementary Figure S3A, lanes 6–8) (13). As shown in Figure 3B (lane 1 versus 7–10), limiting concentrations of δ_2 did not affect transcription of P_ω. Meanwhile, stoichiometric and saturating concentrations of δ_2 inhibited P_ω utilization (2.8- to 3.5-fold). Ultimately utilization was blocked entirely.

To unravel the mechanism of δ_2-mediated P_ω repression, $KMnO_4$ cleavage experiments were performed. Pre-incubation of P_ω DNA with sub-stoichiometric to stoichiometric concentrations of δ_2 followed by addition of RNAP-σ^A did not alter the pattern of $KMnO_4$ cleavage obtained in the absence of δ_2 (Supplementary Figure S5, lanes 1–4 versus 5). This result suggested that δ_2 represses P_ω (Figure 3, lanes 9–10) through gene silencing, i.e. halting RNAP elongation (Figure 3, lanes 9–10). The same model has been as proposed for other ParAB systems to which δ_2 and ω_2 belong (36,37). This model is also consistent with the observation that non-specific binding of δ_2 to DNA might occlude RNAP-σ^A clearance or affect RNAP mediated elongation.

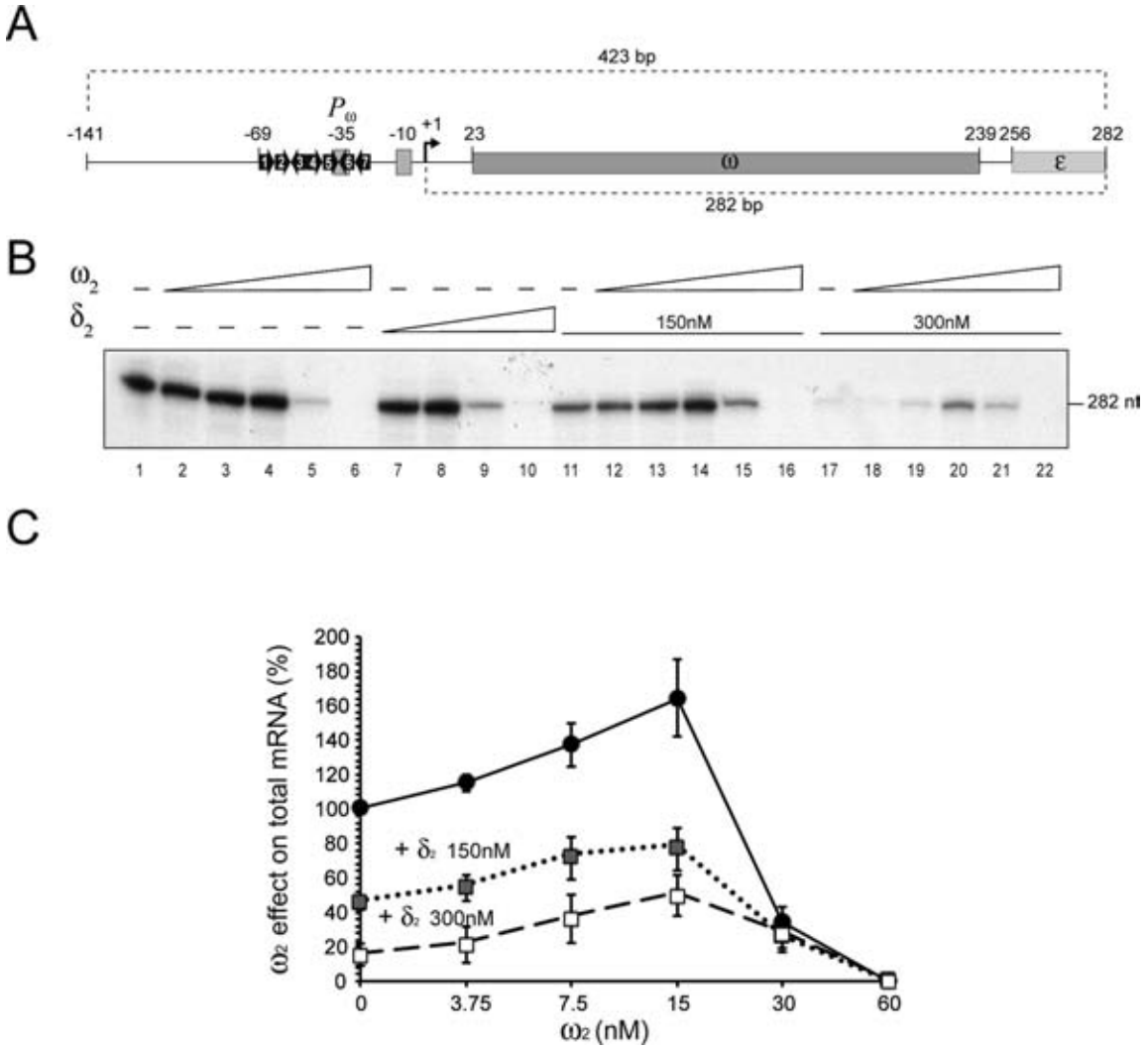

Figure 3. RNAP-σ^A mediated transcription as a function of the presence or absence of ω_2 and δ_2. (**A**) A 423-bp DNA segment containing P_ω is depicted. The heptads are labelled and their relative orientations are represented by arrows. The positions of the −35 and −10 elements are indicated with filled rectangles. The transcription start site is represented with a solid arrow bent 90°. The ω and part of the ϵ gene are indicated as well. (**B**) Run-off experiments: the 423-bp P_ω DNA (5 nM) was the template in an *in vitro* transcription experiment using [α^{32}P]-UTP in buffer C. RNAP-σ^A (20 nM) was present in all cases. Results shown for transcription in the absence (lane 1) or presence of increasing concentrations of either ω_2 (3.7, 7.5, 15, 30 and 60 nM, lanes 2–6) or δ_2 (37, 75, 150, 300 nM, lanes 7–10). Also shown are results of assays in the presence of either 150 or 300 nM δ_2 (lanes 11–16 or 17–22 respectively) with increasing concentrations of ω_2. (**C**) Quantification of mRNA synthesis in the presence of increasing concentrations ω_2 alone or in the presence of a fix concentration of δ_2 (150 or 300 nM). Shown here are the analysed results from five independent experiments.

Protein δ_2 acts as a co-activator of P_ω expression

Upon coming into contact with $\omega_2 \cdot P_\omega$ complexes, δ_2 protein bound to non-specific DNA relocates onto $\omega_2 \cdot P_\omega$ to form ternary C3 complexes (Figure 1E, condition 3) (12). The C3 complex is characterized by a longer half-life than is C1 ($\omega_2 \cdot P_\omega$ DNA). To test whether C3 might affect transcription, P_ω run-off experiments were performed (Figure 3B, lanes 11–22). At 150 nM, a concentration of δ_2 equivalent to its K_{Dapp}, addition of limiting concentrations of ω_2 (1.8 to 3.7 ω_2/P_ω DNA) significantly stimulated mRNA synthesis by >3-fold (Figure 3B, lanes 12–14 and 3C). Nevertheless, synthesis was attenuated and ultimately blocked at higher concentrations of ω_2 (Figure 3B, lanes 15–16).

At 300 nM, δ_2 significantly reduced P_ω utilization by ∼14-fold (Figure 3B, lanes 1 versus 17). Addition of limiting concentrations of ω_2 (1.8–3.7 ω_2/P_ω DNA or 0.2–0.5 ω_2/heptad) significantly stimulated P_ω dependent mRNA synthesis by >6-fold (Figure 3B, lanes 18–20, and 3C). As expected, ω_2 blocked P_ω utilization when used at the slightly saturating concentrations of 15 ω_2/P_ω DNA (Figure 3B, lane 22). It is likely, therefore, that whether ω_2 acts as a transcriptional activator or a repressor hinges on its concentration (Figure 3C). Moreover, while by itself repressing P_ω utilization, δ_2 apparently behaves as a transcriptional co-activator. This is consistent with the observations that: i) the half-life of $\omega_2 \cdot P_\omega$ complex increased ∼30-fold in the presence of δ_2 (10,13); and ii) upon interacting with δ_2, ω_2 bound to P_ω DNA, a rearrangement of its unstructured NTD occurs (see 15).

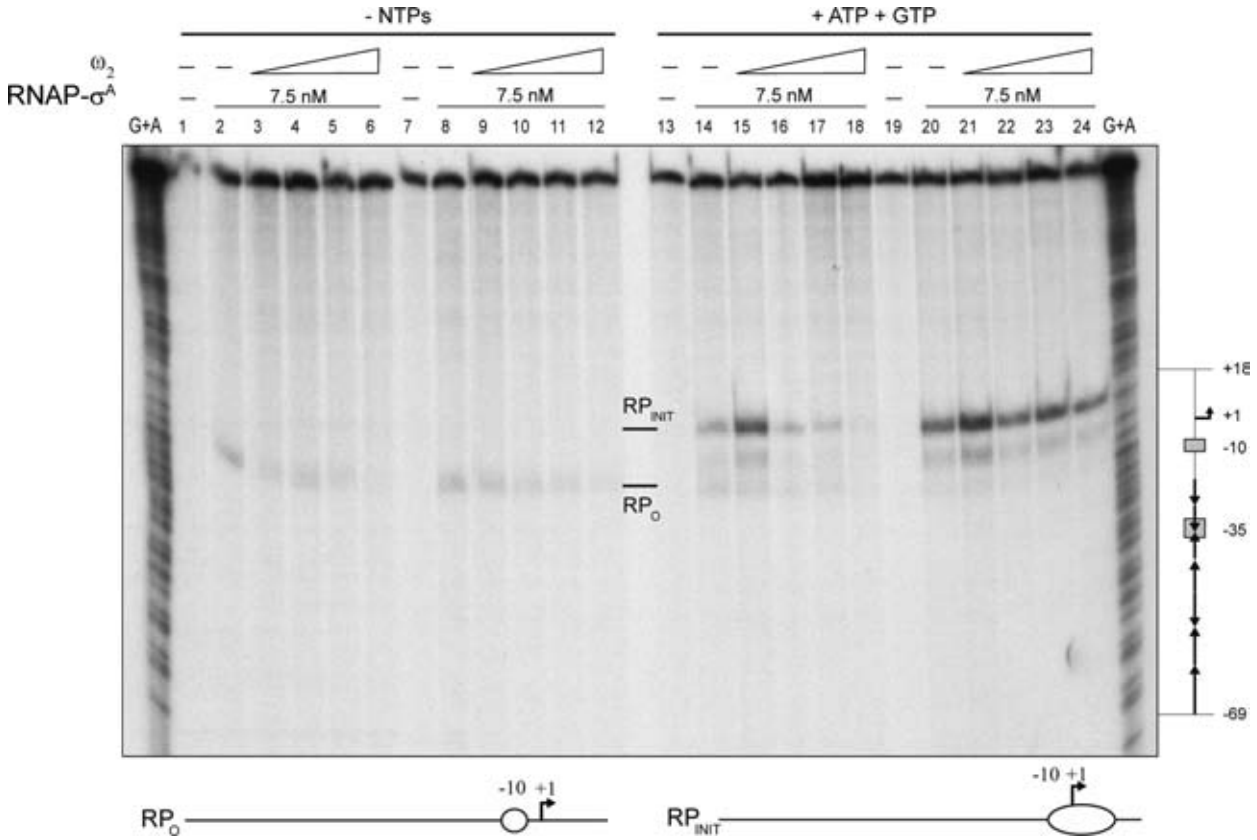

Figure 4. Effect of ω_2 on the formation of RP_O at P_ω. The 423-bp [α^{32}P]-P_ω DNA (1 nM) was pre-incubated with increasing concentrations of ω_2 (7.5, 15, 30 and 60 nM; lanes 2–6 and 14–18) or with 7.5 nM RNAP-σ^A (lanes 8–12 and 20–24) in buffer C. A second protein was added along with the initiating nucleotides, GTP and ATP (as indicated). DNA melting was probed by $KMnO_4$ footprinting as a way of observing the open complex. The positions hypersensitive to $KMnO_4$ are labelled (RP_O and RP_{INIT}) and depicted at the bottom of the figure. The coordinates are relative to the transcription start point. Chemical sequencing reactions for purines (G +A) are shown and the relevant regions of P_ω depicted to the right of the figure.

Protein ω_2 interacts with the NH_2-terminal half of the RNAP-σ^A β' subunit

RNAP-σ^A and ω_2 cooperatively bind P_ω DNA cooperatively and create higher-order nucleoprotein complexes that reflect the combinatorial control of gene expression (Figures 2–4). This effect is likely attributed to direct protein–protein interactions between adjacent DNA-binding factors that promote the assembly of higher-order complexes. To determine whether or not RNAP-σ^A and ω_2 physically interacted, RNAP-σ^A was bound to a Ni^{2+} agarose column through coordination with the C-terminal histidine tag of its β' subunit (30). The RNAP-σ^A-bound matrix retained ω_2, even in the absence of P_ω DNA. These proteins also co-eluted from the matrix during an elution step (Supplementary Figure S6).

Initial identification of the RNAP-σ^A subunit(s) responsible for association to ω_2 was achieved by carrying out far-western blots of RNAP-σ^A, ω_2 and BSA as control. These proteins were resolved by SDS-PAGE under conditions under which the small ω protein (7.9 kDa) migrated with the front. After renaturation of prey proteins and a membrane blocking step, the bait, ω_2, was added. Protein–protein interactions were detected using anti-ω_2 polyclonal antibodies. As expected, ω_2 interacted with itself and also with the co-migrating β and/or β' subunits of RNAP-σ^A. No other subunits gave a signal (Figure 5A). Due to a similarity in mass, β (133.6 kDa) and β' (134.2 kDa) subunits could not be distinguished. We therefore took advantage of the fact that all *B. subtilis* RNAP-σ^A subunits, except for β' (pI 8.8), have acidic pIs and repeated the far-western experiments, this time using two-dimensional (2D)-PAGE. Protein ω_2 interacted with β' and several proteins in unexpected spots (termed 1–2, 3–4 and 5). These had masses of ∼34 kDa and were located in the basic region of the gel (Figure 5B, Ab-anti ω_2 condition). Corresponding polypeptides were extracted from the gel, subjected to mass spectrometry analysis, and identified as RNAP-σ^A β' subunit NTDs with slight variations in the C-termini (Figure 5C). Taking into account the sizes observed, it was assumed that the Sw2 structural module (residues 316–342) was missing from these NTD variants of the β' subunit.

The central and C-terminal regions of ω_2 appears not to interact with RNAP-σ^A

The ω_2 protein has three functional regions: (i) the unstructured NTD (residues 1–24), which is essential for the $\omega_2 \cdot \delta_2$ interaction (11,15); (ii) the β-sheet domain (residues 28–32), which is required for ω_2 recognition of its cognate DNA site (9,14); and (iii) the α-helix α1 (residues 34–46) which, in concert with the α2 helix (residues 51–64) contributes to

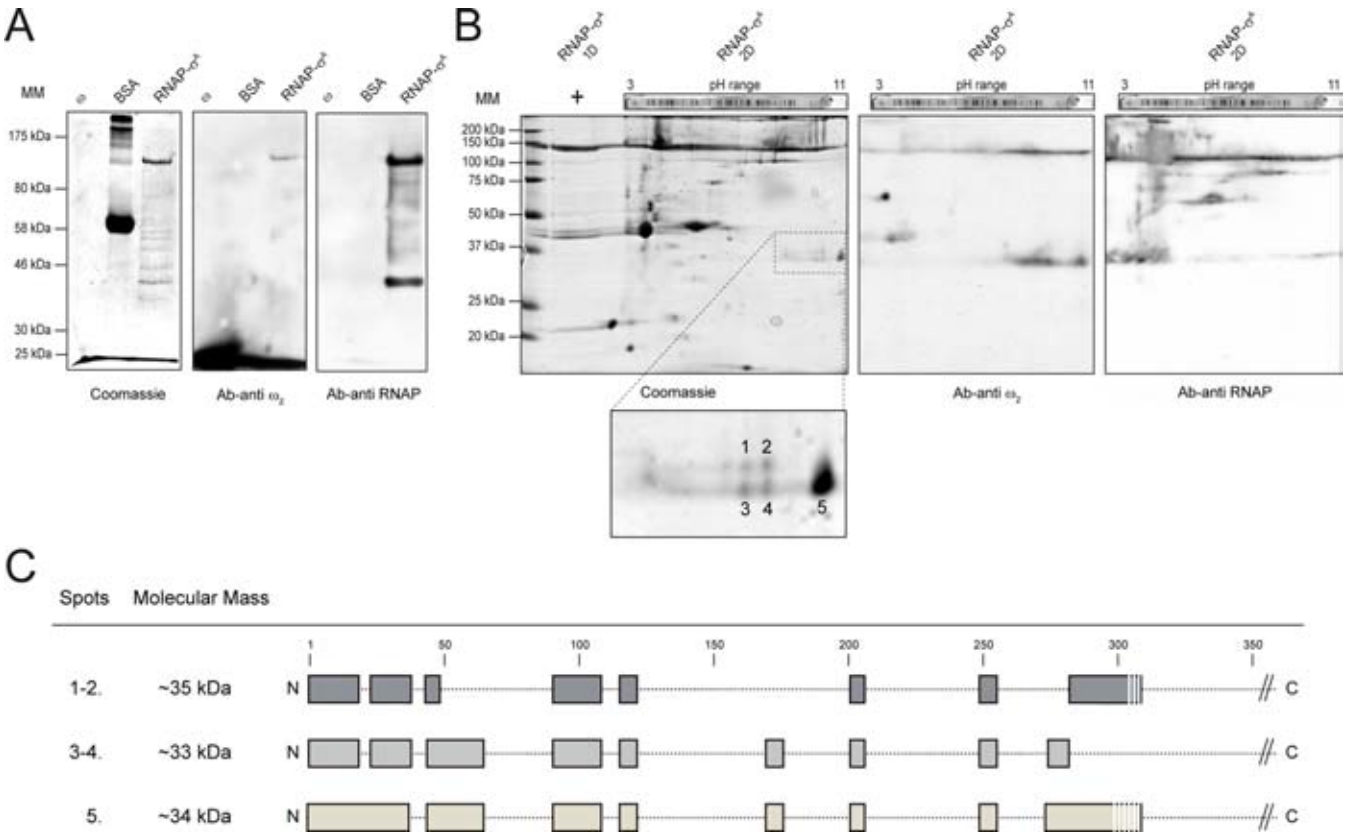

Figure 5. Far-western blotting of ω_2 and RNAP-σ^A. (**A**) 1 μg ω_2, 1 μg RNAP-σ^A or 5 μg BSA (as control) were resolved by SDS-PAGE and either stained with Coomasie blue or transferred onto nitrocellulose membranes. Membranes underwent a renaturing step and incubated with the specific ω_2 and RNAP-σ^A antibodies (Ab). (**B**) 1 μg RNAP-σ^A was resolved by iso-electric focusing in a pH 3–11 gradient followed by an SDS-PAGE. Protein was then transferred to a membrane, renatured, incubated with the ω_2 bait and highlighted with either Ab-anti ω_2 or Ab-anti RNAP-σ^A. (**C**) Basic, ∼34 kDa polypeptides (1–5) that had reacted with Ab-anti ω_2 were gel purified and identified by mass spectrometry. The regions identified are shown in this figure. The sequence coverage was > 40%.

monomer-monomer and dimer-dimer interfaces (8,9). The function, if any, of the C-terminal region (residues 65–71) is unknown (7,8).

Significantly, the 79-residue long ω2 (9.0 kDa) shares a 98% identity with the 71-residue ω for the first 55 residues (Supplemental material Annex 2). However, they only share an 18% identity in the last 24 residues (Supplementary Figure S7A). The ω2 protein repressed P_δ utilization *in vivo* nearly as efficiently as wt ω_2 (Supplemental material Annex 2, Supplementary Figure S7B). Similar results were observed when the P_δ-*lacZ* fusion was replaced by the P_ω-*lacZ* fusion (data not shown). Furthermore, plasmid-borne ω2 and δ genes which were transcribed from P_ω (*parS*2) and P_δ (*parS*1) (Figure 1A), were necessary and sufficient for stabilizing of an otherwise unstable plasmid in *B. subtilis* cells (38, our unpublished results). It is likely that: (i) the dimer is the functional unit of ω2; (ii) $\omega_2$2 interacts with δ_2 just like ω_2; and (iii) the different C-terminal domains of ω and ω2 are not involved in gene repression.

Protein docking experiments predicted that the unstructured ω NTD folded into an α-helical structure that interacted with the β' NTD of RNAP-σ^A (Supplementary Figure S8). In contrast, several charged amino acids located in the coiled region between the α-helices α1 and α2 (residues 47–52) and in the α2 helix itself (residues 51–64) could make contacts with the oppositely charged residues in the β' subunit of RNAP-σ^A. To test this hypothesis (Supplemental material Annex 3), the charged residues that were accessible in these domains, K52, E53, D56, R64 and K70, were replaced with alanine. Subsequently, the *in vivo* behaviour of these mutants was investigated (Supplemental material Annex 3). With the exception of ωD56A, the ω mutant variants repressed P_δ transcription *in vivo* as efficiently as wt ω_2 (Supplementary Figure S7B) (Supplemental material Annex 3). The D56A mutant only reduced P_δ transcription ∼6-fold. As described in Supplementary Annex 3, purified ωD56A also formed dimers, albeit in a far smaller proportion than wt ω_2 (Supplementary Figure S7C). Since in the dimeric form of ω, the β-sheet domain adopts an antiparallel configuration before binding P_ω, the primary defect of ωD56A might be a poor ability to dimerize. Therefore, it was not further analysed. It would be very interesting to determine whether or not the ω_2 NTD can, by itself recruit RNAP-σ^A to the $\omega_2 \cdot P_\omega$ DNA complex.

DISCUSSION

Direct contacts between ω_2 and RNAP-σ^A stimulate RP_C complex formation and its subsequent isomerization to RP_O. This appears to be the mechanism by which limiting

concentrations of ω_2 activate P_ω transcription. This process is further enhanced by δ_2 (Figure 3B). However, stoichiometric concentrations of ω_2 have the opposite effect: here the recruited RNAP-σ^A inefficiently isomerizes into RP_O and represses P_ω or P_δ transcription both *in vivo* and *in vitro*. It would be highly interesting to determine whether or not ω_2 functions as an activator to repressor switch of P_{copS}. However, preliminary results indicate that $\omega_2 \cdot P_{copS}$ DNA forms a ternary complex with RNAP-σ^A and that ω_2 regulates transcription through a mechanism that does not exclude the RNAP-σ^A from the RP_C (4).

The dual activity of the ω_2 regulator

Plasmid-encoded ω_2, from Gram-positive cocci, is the only one out of the more than 2000 RHH_2 proteins that can either activate or repress the utilization of a single promoter (P_ω) in a concentration-dependent manner. This is true at least in a simplified *in vitro* system. The majority of RHH_2 proteins are predicted to be transcriptional repressors (39). However, four of them act both as activators and as repressors. These are: a P22-Arc variant, Mer, AmrZ [AlgZ] and NikR. They bind to a variety of promoters, functioning as repressors for some while behaving as activators for others (40–43). In the case of other putative regulators, various metal cofactors and different stoichiometries might also influence the effect they have on promoter functioning (40–43).

The activator to repressor switch function of ω_2 appears to be managed by the diverse modes of ω_2 binding to the operator region of P_ω. These modes of binding have distinct effects on the initial activity of RNAP-σ^A. Under limiting concentrations, ω_2 promotes RNAP-σ^A binding to operator sequences that overlap the −35 sequence. This results in the stimulation of RP_C formation and in an increase in the rate of isomerization from RP_C to RP_O. It is thus likely that: (i) ω_2 increases the local concentration of both proteins, leading to a ternary $\omega_2 \cdot P_\omega \cdot$RNAP-$\sigma^A$ complex; (ii) this ternary complex facilitates the rate of isomerization from RP_C to RP_O and increases P_ω dependent mRNA synthesis; and (iii) δ_2 may act as a co-activator by increasing the half-life of $\omega_2 \cdot P_\omega$ DNA complexes (see 13).

With stoichiometric concentrations of ω_2 full operator occupancy was achieved, and a different outcome was observed. Under these conditions, ω_2 assembles into a left-handed matrix that wraps around right-handed, straight P_ω DNA (see Figure 1B). This assembly makes P_ω DNA accessible to RNAP-σ^A (RP_C formation), while simultaneously inhibiting isomerization to RP_O (transcriptional repression) (Figure 4, lanes 17–18). *In vitro*, we observed that δ_2 contributed to P_δ repression (Figure 3B), and the presence of both ω_2 and δ_2 transcriptional repression of P_δ and P_ω was elevated *in vivo* with respect to wt ω_2 alone (Supplementary Figure S7B, data not shown). When stoichiometric concentrations of ω_2 were added to preformed RP_O complexes, a moderate effect on P_ω utilization was observed (see Figures 3 and 4). This suggested that RNAP-σ^A transcription was influenced by ω_2 that was bound to its cognate promoters. In sum, we describe here a previously uncharacterized mechanism of transcription regulation in bacteria belonging to the phylum Firmicutes.

Several different models can be considered in order to explain the specific transcriptional repression resulting from the full occupancy of the operator sequences by ω_2: (i) relocation of RNAP-σ^A to a position unfavourable for efficient RP_O formation; (ii) 'locking' RNAP-σ^A into a conformation unfavourable for RP_O formation; (iii) blocking the interaction between the β' NTD and the DNA, which may be an essential step for RP_O formation; and (iv) inhibition of RNAP-σ^A mediated transcription by hindering any putative upstream element. We favour the first model because RP_C formation is stimulated by the interaction between ω_2 and RNAP-σ^A, while the subsequent isomerization step producing stable RP_O (through the unstable intermediate, RP_I) becomes inhibited. Also consistent with this model is the fact that ω_2 establishes interactions with operator sites when RNAP-σ^A is already bound to P_ω DNA. Meanwhile, ω_2 fails to inhibit pre-formed RP_O, Also in line with this model is the observation that, in the presence of limiting amounts of ω_2 bound to P_ω DNA, RNAP-σ^A moves onto P_ω DNA (Supplementary Figure S2A), and that while under saturating concentrations of ω_2, RNAP-σ^A moves off of P_ω DNA (Supplementary Figure S2B).

The interplay between the ω_2 regulator and the β' subunit of RNAP holoenzyme

The work presented here establishes that ω_2 is a global regulator of plasmid biology through its effect on replication, faithful partitioning and better-than random segregation (see Introduction). Importantly, ω_2 represents an exception to the accepted prokaryotic transcription regulation paradigm, which asserts that, there are proteins that can act as either activators or repressors, but that the same protein cannot act as both. Since ω_2 regulates the expression of plasmid encoded genes that are harboured in different Firmicutes bacteria, it presumably recognizes the RNAP β' NTD of all of them. This recognition might be limited to the first 316 amino acids, the length of the shortest polypeptide of the β' subunit that binds ω_2 (Figure 5B). This would not be surprising because the β' subunits of all Firmicutes share a high degree of sequence identity. Consistent with this, ω_2 does not regulate transcription of a genetically distant bacterium (e.g. *E. coli*) (16). These facts imply that the regions of the Firmicutes β' subunits that show a significant degree of sequence divergence are not involved in ω_2 binding, such as residues 124–165 and 178–208 (22% and 13%, respectively). Presumably, residues 260–271, which match almost perfectly between the β' subunits of *E. coli* and *B. subtilis*, is a region also not involved in ω_2 binding.

Few proteins have been observed to interact with the RNAP β' subunit. Most of these are encoded by proteobacterial phages. The phage Xp10-p7 factor interacts with the first 10 residues of the NTD of β' (44). The Mu-C protein binds to part of region F (b7) (45). T7-Gp2 recognizes part of the jaw (b9-b10) and σ 1.1 domains (46,47). And lastly, N4-SSB interacts with part of region H (b11) at the CTD (48). These regulators do not share a specific target domain and have different modes of action: N4-SSB and Mu-C specifically act as transcription activators (45,48), while T7-Gp2 and Xp10-p7 are repressors (44,46). In contrast, ω_2 has a dual function (Figure 3B). Of these regulators,

only T7-Gp2, Xp10-p7, and ω_2 act during the early stages of RNAP-σ isomerization. Meanwhile, T7-Gp2 and Xp10-p7 directly interact with RNAP-σ rather than binding to *P* DNA as does ω_2 (44,46,47).

Biological implication of ω_2-mediated transcription regulation

A growing number of plasmid-encoded genetic determinants for resistance to diverse antimicrobials among streptococci, enterococci and staphylococci has been shown to be regulated by ω-like cofactors. They act either as part of the ωεζ operon or on their own as part of the ω cassette (ω or ω2 genes) (1). In conjunction with δ_2 and RNAP-σ, the biological role of ω_2 as a dual regulator is to control vital plasmid functions in Firmicutes. It corrects the downward fluctuations in plasmid copy number through regulation of the synthesis of CopS (also termed CopF, CopR). CopS is a repressor of the initiator RepS (also termed RepE, RepR) protein. ω_2 also controls the synthesis of the toxin-antitoxin module, which in turn restricts the survival of plasmid-free segregants. The ω_2 protein mediates the synthesis of the partition system by regulating the expression of δ_2 and ω_2. Protein $\omega_2$2 manages the expression of the *ermB* gene (4,16,49). With the help of δ_2 (the ParA ATPase), the ω_2 (the ParB centromere binding) protein also safeguards plasmid faithful segregation via the ParAB system. The regulation of Firmicutes RNAP-σ^A by the ω cassette is a newly characterized mechanism through which bacterial transcription of a large number of antibiotic resistance genes is regulated.

SUPPLEMENTARY DATA

Supplementary Data are available at NAR Online.

ACKNOWLEDGEMENT

We thank Margarita Salas and José M Lazaro for their generous gift of rabbit polyclonal anti-RNAP-σ^A. This work was supported in part by grant BFU2012–39879-C02-01 awarded to J.C.A by the Dirección General de Investigación-Ministerio de Economía y Competitividad (DGI-MINECO). A.V. thanks the Consejería de Educación de la Comunidad de Madrid for its fellowship (CPI/0266/2008) and the European Social Fund (ESF). M.T. is a PhD fellow supported by the La Caixa Foundation International Fellowship Programme of La Caixa/CNB.

FUNDING

Funding for open access charge: Dirección General de Investigación-Ministerio de Economía y Competitividad [BFU2012-39879-C02-01 to J.C.A.].
Conflict of interest statement. None declared.

REFERENCES

1. Volante,A., Soberón,N.E., Ayora,S. and Alonso,J.C. (2014) The interplay between different stability systems contributes to faithful segregation: *Streptococcus pyogenes* pSM19035 as a model. *Microbiol. Spectrum.*, **2**, PLAS-0007.
2. Croucher,N.J., Harris,S.R., Fraser,C., Quail,M.A., Burton,J., van der Linden,M., McGee,L., von Gottberg,A., Song,J.H., Ko,K.S. *et al.* (2011) Rapid pneumococcal evolution in response to clinical interventions. *Science*, **331**, 430–434.
3. Camacho,A.G., Misselwitz,R., Behlke,J., Ayora,S., Welfle,K., Meinhart,A., Lara,B., Saenger,W., Welfle,H. and Alonso,J.C. (2002) *In vitro* and *in vivo* stability of the $\epsilon_2\zeta_2$ protein complex of the broad host-range *Streptococcus pyogene*s pSM19035 addiction system. *Biol. Chem.*, **383**, 1701–1713.
4. de la Hoz,A.B., Ayora,S., Sitkiewicz,I., Fernandez,S., Pankiewicz,R., Alonso,J.C. and Ceglowski,P. (2000) Plasmid copy-number control and better-than-random segregation genes of pSM19035 share a common regulator. *Proc. Natl. Acad. Sci. U.S.A.*, **97**, 728–733.
5. Dmowski,M., Sitkiewicz,I. and Ceglowski,P. (2006) Characterization of a novel partition system encoded by the δ and ω genes from the streptococcal plasmid pSM19035. *J. Bacteriol.*, **188**, 4362–4372.
6. Lioy,V.S., Pratto,F., de la Hoz,A.B., Ayora,S. and Alonso,J.C. (2010) Plasmid pSM19035, a model to study stable maintenance in Firmicutes. *Plasmid*, **64**, 1–17.
7. Murayama,K., de la Hoz,A.B., Alings,C., Lopez,G., Orth,P., Alonso,J.C. and Saenger,W. (1999) Crystallization and preliminary X-ray diffraction studies of *Streptococcus pyogenes* plasmid pSM19035-encoded ω transcriptional repressor. *Acta Crystallogr. D Biol. Crystallogr.*, **55**, 2041–2042.
8. Murayama,K., Orth,P., de la Hoz,A.B., Alonso,J.C. and Saenger,W. (2001) Crystal structure of ω transcriptional repressor encoded by *Streptococcus pyogenes* plasmid pSM19035 at 1.5 A resolution. *J. Mol. Biol.*, **314**, 789–796.
9. Weihofen,W.A., Cicek,A., Pratto,F., Alonso,J.C. and Saenger,W. (2006) Structures of ω repressors bound to direct and inverted DNA repeats explain modulation of transcription. *Nucleic Acids Res.*, **34**, 1450–1458.
10. de la Hoz,A.B., Pratto,F., Misselwitz,R., Speck,C., Weihofen,W., Welfle,K., Saenger,W., Welfle,H. and Alonso,J.C. (2004) Recognition of DNA by ω protein from the broad-host range *Streptococcus pyogenes* plasmid pSM19035: analysis of binding to operator DNA with one to four heptad repeats. *Nucleic Acids Res.*, **32**, 3136–3147.
11. Welfle,K., Pratto,F., Misselwitz,R., Behlke,J., Alonso,J.C. and Welfle,H. (2005) Role of the N-terminal region and of β-sheet residue Thr29 on the activity of the ω_2 global regulator from the broad-host range *Streptococcus pyogenes* plasmid pSM19035. *Biol. Chem.*, **386**, 881–894.
12. Pratto,F., Suzuki,Y., Takeyasu,K. and Alonso,J.C. (2009) Single-molecule analysis of protein·DNA complexes formed during partition of newly replicated plasmid molecules in *Streptococcus pyogenes*. *J. Biol. Chem.*, **284**, 30298–30306.
13. Soberón,N.E., Lioy,V.S., Pratto,F., Volante,A. and Alonso,J.C. (2011) Molecular anatomy of the *Streptococcus pyogenes* pSM19035 partition and segrosome complexes. *Nucleic Acids Res.*, **39**, 2624–2637.
14. Dostál,L., Pratto,F., Alonso,J.C. and Welfle,H. (2007) Binding of regulatory protein ω from *Streptococcus pyogenes* plasmid pSM19035 to direct and inverted 7-Base pair repeats of operator DNA. *J. Raman Spectrosc.*, **38**, 166–175.
15. Volante,A. and Alonso,J.C. (2015) Molecular anatomy of ParA-ParA and ParA-ParB interactions during plasmid partitioning. *J. Biol. Chem.*, **290**, 18782–18795.
16. Pratto,F., Cicek,A., Weihofen,W.A., Lurz,R., Saenger,W. and Alonso,J.C. (2008) *Streptococcus pyogenes* pSM19035 requires dynamic assembly of ATP-bound ParA and ParB on parS DNA during plasmid segregation. *Nucleic Acids Res.*, **36**, 3676–3689.
17. Record,M. Jr, Reznikoff,W., Craig,M., McQuade,K. and Schlax,P. (1996) In: Neidhardt,F, Curtiss,RI, Ingraham,J, Lin,E, Low,K, Magasanik,B, Reznikoff,W, Riley,M, Schaechter,M and Umbarger,H (eds). *In Escherichia coli and Salmonella: Cellular and Molecular Biology*. 2nd Edn. ASM Press, Washington, DC, pp. 792–821.
18. Vassylyev,D.G., Vassylyeva,M.N., Perederina,A., Tahirov,T.H. and Artsimovitch,I. (2007) Structural basis for transcription elongation by bacterial RNA polymerase. *Nature*, **448**, 157–162.
19. Lane,W.J. and Darst,S.A. (2010) Molecular evolution of multisubunit RNA polymerases: structural analysis. *J. Mol. Biol.*, **395**, 686–704.

20. Zhang,Y., Feng,Y., Chatterjee,S., Tuske,S., Ho,M.X., Arnold,E. and Ebright,R.H. (2012) Structural basis of transcription initiation. *Science*, **338**, 1076–1080.
21. Darst,S.A. (2001) Bacterial RNA polymerase. *Curr. Opin. Struct. Biol.*, **11**, 155–162.
22. Murakami,K.S. and Darst,S.A. (2003) Bacterial RNA polymerases: the wholo story. *Curr. Opin. Struct. Biol.*, **13**, 31–39.
23. Gruber,T.M. and Gross,C.A. (2003) Multiple σ subunits and the partitioning of bacterial transcription space. *Annu. Rev. Microbiol.*, **57**, 441–466.
24. Ebright,R.H. (2000) RNA polymerase: structural similarities between bacterial RNA polymerase and eukaryotic RNA polymerase II. *J. Mol. Biol.*, **304**, 687–698.
25. Haugen,S.P., Ross,W. and Gourse,R.L. (2008) Advances in bacterial promoter recognition and its control by factors that do not bind DNA. *Nat. Rev. Microbiol.*, **6**, 507–519.
26. Murakami,K.S., Masuda,S., Campbell,E.A., Muzzin,O. and Darst,S.A. (2002) Structural basis of transcription initiation: an RNA polymerase holoenzyme-DNA complex. *Science*, **296**, 1285–1290.
27. Vassylyev,D.G., Sekine,S., Laptenko,O., Lee,J., Vassylyeva,M.N., Borukhov,S. and Yokoyama,S. (2002) Crystal structure of a bacterial RNA polymerase holoenzyme at 2.6 Å resolution. *Nature*, **417**, 712–719.
28. Saecker,R.M., Record,M.T. Jr and Dehaseth,P.L. (2011) Mechanism of bacterial transcription initiation: RNA polymerase - promoter binding, isomerization to initiation-competent open complexes, and initiation of RNA synthesis. *J. Mol. Biol.*, **412**, 754–771.
29. Browning,D.F. and Busby,S.J. (2004) The regulation of bacterial transcription initiation. *Nat. Rev. Microbiol.*, **2**, 57–65.
30. Fujita,M. and Sadaie,Y. (1998) Rapid isolation of RNA polymerase from sporulating cells of *Bacillus subtilis*. *Gene*, **221**, 185–190.
31. Miller,J.H. (1972) *Experiments in Molecular Genetics*, Cold Spring Harbor Lab. Press, Plainview, NY.
32. Zechel,K. (1977) On the resolution of polypeptides by isoelectric focusing in polyacrylamide gels in the presence of urea and nonidet-p40. *Anal. Biochem.*, **83**, 240–251.
33. Wu,Y., Li,Q. and Chen,X.Z. (2007) Detecting protein-protein interactions by Far western blotting. *Nat. Protoc.*, **2**, 3278–3284.
34. Lioy,V.S., Martin,M.T., Camacho,A.G., Lurz,R., Antelmann,H., Hecker,M., Hitchin,E., Ridge,Y., Wells,J.M. and Alonso,J.C. (2006) pSM19035-encoded ζ toxin induces stasis followed by death in a subpopulation of cells. *Microbiology*, **152**, 2365–2379.
35. Tapias,A., Fernandez,S., Alonso,J.C. and Barbe,J. (2002) *Rhodobacter sphaeroides* LexA has dual activity: optimising and repressing *recA* gene transcription. *Nucleic Acids Res.*, **30**, 1539–1546.
36. Rodionov,O., Lobocka,M. and Yarmolinsky,M. (1999) Silencing of genes flanking the P1 plasmid centromere. *Science*, **283**, 546–549.
37. Lynch,A.S. and Wang,J.C. (1995) SopB protein-mediated silencing of genes linked to the *sopC* locus of *Escherichia col*i F plasmid. *Proc. Natl. Acad. Sci. U.S.A.*, **92**, 1896–1900.
38. Lioy,V.S., Volante,A., Soberón,N.E., Lurz,R., Ayora,S. and Alonso,J.C. (2015) ParAB partition dynamics in Firmicutes: nucleoid bound ParA captures and tethers ParB-plasmid complexes. *PLoS One*, **10**, e0131943 .
39. Schreiter,E.R. and Drennan,C.L. (2007) Ribbon-helix-helix transcription factors: variations on a theme. *Nat. Rev. Microbiol.*, **5**, 710–720.
40. Smith,T.L. and Sauer,R.T. (1996) Dual regulation of open-complex formation and promoter clearance by Arc explains a novel repressor to activator switch. *Proc. Natl. Acad. Sci. U.S.A.*, **93**, 8868–8872.
41. Schreiter,E.R., Sintchak,M.D., Guo,Y., Chivers,P.T., Sauer,R.T. and Drennan,C.L. (2003) Crystal structure of the nickel-responsive transcription factor NikR. *Nat. Struct. Biol.*, **10**, 794–799.
42. Muller,C., Bahlawane,C., Aubert,S., Delay,C.M., Schauer,K., Michaud-Soret,I. and De Reuse,H. (2011) Hierarchical regulation of the NikR-mediated nickel response in *Helicobacter pylori*. *Nucleic Acids Res.*, **39**, 7564–7575.
43. Pryor,E.E. Jr, Waligora,E.A., Xu,B., Dellos-Nolan,S., Wozniak,D.J. and Hollis,T. (2012) The transcription factor AmrZ utilizes multiple DNA binding modes to recognize activator and repressor sequences of *Pseudomonas aeruginosa* virulence genes. *PLoS Pathog.*, **8**, e1002648.
44. Yuzenkova,Y., Zenkin,N. and Severinov,K. (2008) Mapping of RNA polymerase residues that interact with bacteriophage Xp10 transcription antitermination factor p7. *J. Mol. Biol.*, **375**, 29–35.
45. Swapna,G., Chakraborty,A., Kumari,V., Sen,R. and Nagaraja,V. (2011) Mutations in beta' subunit of *Escherichia coli* RNA polymerase perturb the activator polymerase functional interaction required for promoter clearance. *Mol. Microbiol.*, **80**, 1169–1185.
46. James,E., Liu,M., Sheppard,C., Mekler,V., Camara,B., Liu,B., Simpson,P., Cota,E., Severinov,K., Matthews,S. *et al.* (2012) Structural and mechanistic basis for the inhibition of *Escherichia coli* RNA polymerase by T7 Gp2. *Mol. Cell*, **47**, 755–766.
47. Bae,B., Davis,E., Brown,D., Campbell,E.A., Wigneshweraraj,S. and Darst,S.A. (2013) Phage T7 Gp2 inhibition of *Escherichia coli* RNA polymerase involves misappropriation of σ^{70} domain 1.1. *Proc. Natl. Acad. Sci. U.S.A.*, **110**, 19772–19777.
48. Miller,A., Wood,D., Ebright,R.H. and Rothman-Denes,L.B. (1997) RNA polymerase beta' subunit: a target of DNA binding-independent activation. *Science*, **275**, 1655–1657.
49. Lioy,V.S., Machon,C., Tabone,M., Gonzalez-Pastor,J.E., Daugelavicius,R., Ayora,S. and Alonso,J.C. (2012) The ζ toxin induces a set of protective responses and dormancy. *PLoS One*, **7**, e30282.